AIAA JOURNAL
Vol. 41, No. 11, November 2003

Effect of Temperature on the Process of Hypervelocity Gouging

David J. Laird* and Anthony N. Palazotto†
U.S. Air Force Institute of Technology, Wright–Patterson Air Force Base, Ohio 45433-7765

The sliding interface of a flyer/target system is subject to immense forces caused by dynamic loads and impact of the flyer with the target. In addition, tremendous heating caused by aerodynamic and frictional effects is produced at the interface. The buildup of the temperature caused by external heat sources is important for an understanding of any impact environment between the flyer and the target. Under these severe loading conditions the material in both the flyer and the target will experience large unstable nonlinear deformations known as gouging. To successfully model the gouging phenomenon, the tangential impact and thermal heating caused by aerodynamic flow and frictional heating must be properly handled. Previous gouging analysis has not accounted for thermal profiles present in the system prior to impact. The hydrocode CTH is employed to solve the gouging problem through the proper modeling of the applicable physics. Results of simulated gouges at elevated temperatures are presented along with a discussion of the mechanics involved and the influence of elevated temperature states.

Introduction

IN fields dealing with hypervelocity sliding, a damage mechanism known as *gouging* can occur under certain loading conditions. Gouging is a failure mode found in metals undergoing hypervelocity sliding contact and is characterized by the permanent deformation and damage of a target caused by the sliding impact of a flyer. At hypersonic speeds the impact of the flyer on the target can cause a teardrop shape of material (Fig. 1) to be gouged away from the surface of each material in a matter of microseconds.

A facility experiencing particular problems with gouging is the Holloman High Speed Test Track (HHSTT) facility at Holloman Air Force Base, New Mexico. This is a ground-based test facility designed to test items under simulated free-flight conditions. Testing is conducted using rocket-propelled sled vehicles guided by steel slippers that ride on continuous steel rails. Currently, users of the facility have requirements to conduct tests at up to 3 km/s (10,000 fps). To achieve such velocities, a $20 million investigation and engineering effort has been performed to overcome a variety of challenges, including gouging, which often leads to catastrophic system failure. Figure 2 shows a photo of the Super Road Runner rocket with its major parts identified. This sled uses a narrow-gauge dual-rail system (as opposed to wide gauge or monorail configurations) and set the world land speed record of 2.869 km/s (6416 mph) on 30 April 2003. For hypervelocity testing portions of the test track are enclosed in a helium-filled tent to reduce aerodynamic drag and heating.

Gouge development can be described as follows: surface imperfections, whether preexisting or caused by contact, provide some initial deformation of the parallel surfaces. This deformation can locally arrange the materials in such a way as to introduce a normal component of the hypervelocity impact in a small region. Under this condition inertial forces are so great that the materials exhibit fluidlike behavior, and the impact-induced pressure sustains a local region of plasticity. The plastic flow in this area leads to the development of material jets that impinge on each other in a continuous interaction, initiating the gouge. Progressive growth of the material jets will cause the gouge to grow further, ending when the materials are no longer in contact.

Received 3 February 2003; revision received 14 July 2003; accepted for publication 18 July 2003. This material is declared a work of the U.S. Government and is not subject to copyright protection in the United States. Copies of this paper may be made for personal or internal use, on condition that the copier pay the $10.00 per-copy fee to the Copyright Clearance Center, Inc., 222 Rosewood Drive, Danvers, MA 01923; include the code 0001-1452/03 $10.00 in correspondence with the CCC.

*Ph.D. Graduate Professor, Department of Aeronautical and Astronautical Engineering.

†Professor, Department of Aeronautical and Astronautical Engineering. Associate Fellow AIAA.

This development of the gouge is characterized by extreme local deformation, heating, melting, and possibly vaporization. A fluid boundary layer between the materials can be created. Overall, the gouge development can be characterized by fluid-like interaction and mixing of the materials. Some current applications of hypervelocity sliding include rocket sleds, rail guns, and two-stage gas guns.

Because of the extreme loading conditions, large nonlinear deformations, shock-wave propagation, and high strain rates produced in gouging, classical Hamiltonian solution methods are not adequate to model the phenomenon. Furthermore, laboratory and field testing have not yet produced a method of studying the actual development of the gouge and the mechanics involved. Because of these issues, numerical methods are employed to develop techniques that can be used to predict gouging phenomena at velocities up to 3 km/s. Hydrocodes (or hydroram codes) are numerical programs specifically designed for problems involving high energy, explosives, material incompressibility, shock propagation, nonlinear response, and large deformations. Hydrocodes have been used successfully to model high-velocity gouging.[1–5]

Thermal Sources and Effects

Gouging is affected by a combination of conditions, including material properties, velocity, and loading conditions. Heating of the materials involved modifies their material properties, including lowering their yield strengths. Previous research has indicated that decreasing material yield strength lowers the materials resistance to gouging.[4,5] In addition, the presence of a thermal gradient will induce thermal strain, which can also effect gouge development.

Until now, gouging simulations have considered only room-temperature materials. However, in many applications the materials might be at highly elevated temperatures before and during the development of gouging. The buildup of the temperature caused by external heat sources is important for an understanding of any impact environment between the flyer and the target. In a hypervelocity impact scenario there are two primary external heat sources. One source is aerodynamic heating from the flow around the flyer, which for the application of rocket sleds has been studied by Korkegi and Briggs,[6,7] and Lofthouse et al.[8] Airflow around the flyer can produce heating caused by aerodynamic shock compression and viscous boundary-layer flow. If the flyer and target are part of a larger, complex geometry, the components might also be subject to reflected and interacting shock waves that can result in localized severe thermal and structural loads. The other major contribution to heat input is frictional heating caused by sliding contact between the flyer and target. Krupovage and Rassmussen have performed an investigation of hypervelocity frictional heating for the HHSTT.[9] These studies show that the system can be subject to extreme heat and demonstrates

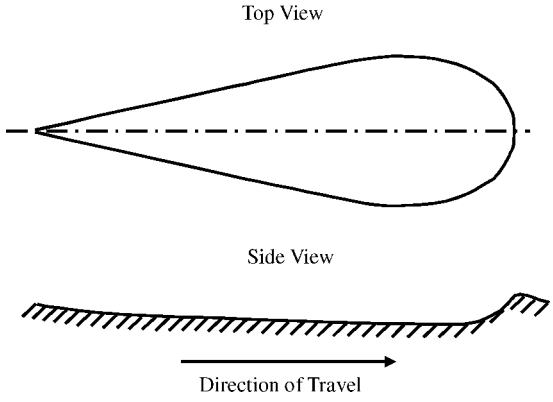

Fig. 1 Gouge representation (U.S. Air Force, H. Newcomb).

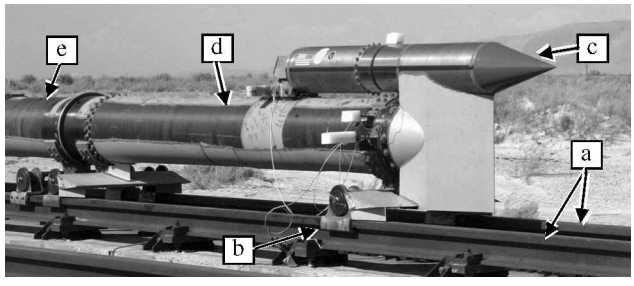

Fig. 2 Super Road Runner (U.S. Air Force photo, H. Newcomb). hypervelocity sled parts: a) guiders (targets), b) slippers (flyers), c) payload, d) third-stage rocket motor, and e) second-stage rocket motor.

the need for the study of temperature effects on the development of gouging. Internally, material shock heating and strain energy will also produce heat. Other heat sources can be present depending on the specific application.

Predicting the Thermal Environment

Even though temperatures at the sliding interfaces between the flyer and target are considerably higher than room temperature, only room temperature has been considered as an environmental condition in previous studies concerning material properties and computational simulations of gouging. No consideration has been given to the effects of elevated temperatures. Raising the material temperatures in the computational model can be used to determine whether gouge initiation and development mechanisms are affected. Elevated temperature solutions can also serve as the basis for further study of the interactive effect of flyer and target materials and can be used to determine if there exists a relationship between flyer properties, gouging onset velocity, and target properties. For example, Mixon[10] attributed the observation that the number of gouges per 100 ft is significantly higher after peak velocity then before to flyer deterioration, but this can also be partly the result of increasing flyer temperature.

In the flyer assembly there are three main sources of heat: the aerodynamic heating from the flow around the flyer (including both stagnation near the leading edge and flow over the contact surface prior to impact), frictional contact between the flyer and target, and oxidation of the materials.

Aerodynamic Heating

The aerodynamic model of the airflow between the flyer and target prior to impact for application to the HHSTT developed by Korkegi and Briggs[6,7] consisted of a laminar stagnation region at the leading edge of the flyer followed by a separate turbulent boundary layer on the flyer and target merging into a Couette flow asymptote. The researchers concluded that the airflow through this gap is shock compressed to high pressures and temperatures resulting in high lift loads and high heat rates to the contact surface of the flyer. They estimated the heat rates and pressure distributions along the gap

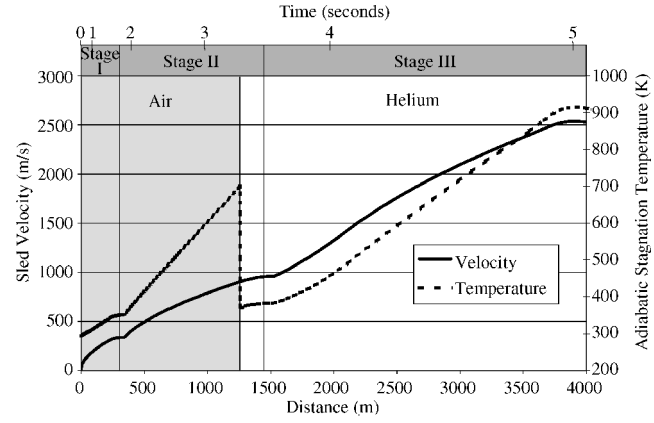

Fig. 3 Sled test velocity profile.[10]

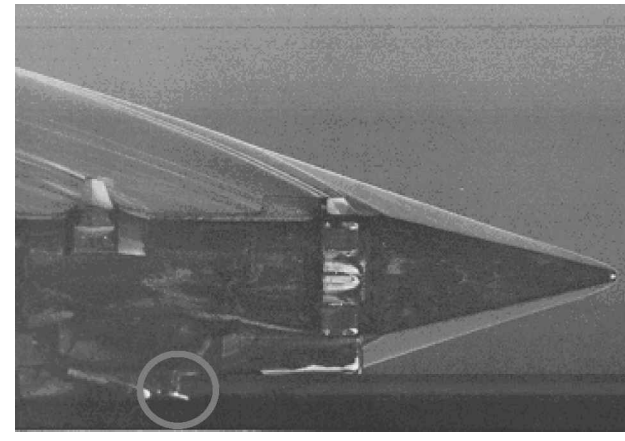

Fig. 4 Shock wave and aerodynamic heating of sled.

from Mach 4 to 10 on the contact surface of the flyer are of the same order as that encountered at the stagnation point of the leading edge on reentry vehicles, a magnitude of about 10^8 J/m^2-s.

At the leading edge of bodies in aerodynamic flow, a point where the airflow changes velocity to match that of the body is known as a stagnation point. At these points the air temperature can increase drastically. An example of a 2.5-km/s sled test profile from the HHSTT is shown in Fig. 3 depicting sled velocity and adiabatic stagnation temperature vs distance traveled and time. The burn periods of the three rocket stages are also shown along with the transition from air to a helium environment. The helium-enclosed section of the track greatly reduces aerodynamic forces and heating and reduces the Mach number from what would have been 10 in air down to Mach 3 in the helium. For this high-speed run a peak stagnation temperature of over 900 K is reached. Figure 4 shows an example of shock waves produced by the hypersonic sled, and the high-temperature stagnation points at component leading edges appear white because of heating. The circled area in this photo is the leading edge of the slipper and gives some indication of the intense heating that is experienced.

Because the HHSTT rail is within 3 ft (0.91 m) of the ground, flow around a dual-rail sled can be trapped between the sled and the trough between the rails.[11] Also, because of the complex geometry preceding the flyer gap the flyer is subject to reflected and interacting shock waves that can result in severe thermal and structural loads.

Frictional Heating

An investigation of the frictional heating by Krupovage and Rassmussen[9] related frictional heating to the energy developed by friction between the flyer and target. They found that the power developed by friction is directly proportional to the material friction coefficient, bearing pressure, and relative velocity. The rate of energy produced by friction is the product of the frictional force and

the sled velocity, where the frictional force can be written as the product of the normal force and coefficient of friction. This empirically determined friction has been shown to be a direct function of the sliding velocity.[9] Thus the frictional heating can be expressed as

$$\dot{w} = C_f N v \tag{1}$$

where $\dot{w}$ is the rate of work (or energy) developed by the sliding friction, N is the normal force, v is the relative velocity, and C_f is the coefficient of friction (which is a function of sliding velocity).

A similar approach to calculate the change in energy at the interface caused by friction considers normal force data from an analysis performed at the HHSTT using a software tool known as DADS (Dynamic Analysis and Design System) from LMS CADSI. DADS is a program that numerically solves the dynamic equations of motion of a system comprised of masses, springs, dampers, and various force elements. The total change in energy in this case will be determined by the frictional force (i.e., $C_f N$) times the distance the flyer moves. We assume that all of this energy is converted to heat (a worst-case assumption because some amount will convert into plastic work and noise), and that half of the energy is transferred into the target and the other half into the flyer. So then the amount of energy imparted to the flyer is

$$\Delta E_{\text{flyer}} = \tfrac{1}{2} w = \tfrac{1}{2} C_f N d \tag{2}$$

Using the definition of specific heat, which is temperature dependent, the change in temperature can be determined by solving for the left-hand side of

$$\int_{T_0}^{T} c_v dT = \frac{\Delta E_{\text{flyer}}}{m} = \frac{C_f N d}{2m} \tag{3}$$

The next several paragraphs describe how numbers were selected to solve Eq. (3). The specific heat of the a flyer made of VascoMax 300 steel is known at four temperatures as shown in Table 1.

A linear fit of these points is used for the expression of c_v integrated in Eq. (3).

The normal force N between the rail and slipper is calculated by DADS using the Hertzian contact formulation of impact theory. Examining DADS data, the average normal force of the final stage over the length of the run is 9200 N. The total distance d of this simulated run is 4171 m.

Although C_f is dependent on velocity and possibly other system parameters, test track engineers have found that using $C_f = 0.1$ provides results with sufficient correlation between DADS predictions and actual results in terms of sled position vs time.

The largest contact area of the flyer is the upper surface, which is 10.16 cm wide by 20.32 cm long. For the given material and a 5-s run time, a time-dependent diffusion study shows that 90% of the thermal energy is contained within 1.27 cm of the thermal source at the surface. If we assume that this depth of steel over the upper surface area absorbs this energy, the mass used in the equation will be 2.1 kg.

With these figures the estimated temperature of the effected mass is 1323 K. If it is considered, however, that only portions of the flyer will be in contact, it is observed from Eq. (3) that lowering effected slipper mass increases the temperature. At the test track the contact surfaces tend to be small at any given time, such as contact along a line. Using the current curve fit for c_v, if one assumes a total contact surface over the run is one-quarter of the area just suggested, the temperature increases to 2595 K above the 2310 K melting point of the material. However, because the specific heat is extrapolated in this temperature range, and because it is difficult to determine how much contact area there really is, this analysis was performed only to get a rough estimate of the flyer temperature and was not carried out with any more fidelity than described.

Table 1 Specific heat of VascoMax 300 steel[19]

Temperature, K	Specific heat c_v, J/gK
298	0.360
422	0.481
598	0.599
700	0.585

Chemical Reactions

At sufficiently high temperatures there are several additional effects that need to be considered to predict the temperature accurately. For air temperatures over 1000 K ($M > 3$) the vibrational energy within the molecules is increased, causing the specific heat of the air to increase with temperature. At higher temperatures, starting at 2500 K ($M > 6$), the molecules begin to dissociate and even ionize, causing the gas to become chemically reactive, and the specific heat becomes a function of both temperature and pressure. The temperature-dependent specific heat yields a gas temperature that is lower than that predicted using the constant specific heat for low temperature. Besides their effect on the gas temperature, chemical reactions can also result in severe erosive oxidation of sled components. Once oxidation is initiated, the additional energy produced by the chemical reaction is usually sufficient to cause complete breakdown and erosion of the material within milliseconds,[9] and the byproducts of such erosion are then also found in the boundary layer. These problems have been greatly alleviated through the use of the helium environment, but are still problematic in track sections or tests where helium is not used.

Many hydrocodes have some capabilities to handle high-energy burn conditions, and these can have applications to the reactive flow around the flyer. However, this scenario is not considered as part of this work.

Numerical Background

Gouging initiates under severe thermal and bearing pressure conditions caused by heating and surface contact of the flyer as it impacts the target. The hydrocode CTH has proven to have the ability to solve adequately the gouging problem.[1–3,5,12,13] CTH and other hydrocodes have a number of nonlinear material models, and equation of state are capable of handling three-dimensional, multimaterial problems.

CTH is a family of codes developed at Sandia National Laboratories for modeling complex multidimensional, multimaterial problems that involve large deformations and strong shocks. A two-step, second-order-accurate Eulerian finite volume solution algorithm is used to solve the mass, momentum, and energy conservation equations. CTH contains models for material strength, fracture, porosity, and high explosive detonation and initiation.[14]

In the gouging problem behavior of the system deformation is a major concern. Therefore, it is important to model properly the materials involved and solve the thermodynamics and material response. Material modeling can be categorized into three areas: the equation of state, the constitutive relations, and failure models.[15]

Equation of State

When shock-wave dynamics are involved, the effects must be related through an equation of state (EOS). The equation of state provides a relationship between pressure, density, internal energy, and entropy of a material. In the hypervelocity regime the form of the equation of state is important in predicting the dynamics, and several forms of the equation of state have been specialized for this purpose. Although simple forms can actually be represented as an equation, tabular models allow the use of sophisticated models that are too complicated to be incorporated into analytic formulas, and a good tabular EOS can give valid results over a much wider density–temperature range than analytic models by considering a number of chemical and physical phenomena that affect material behavior, such as electronic structure, nuclear thermal motion, phase transitions, chemical reactions, and thermal electronic excitation and ionization.[16] For iron and ironlike alloys chart D to the three-halves power (CTH) contains a tabular model developed by Sandia National Laboratories known as the SESAME tabular EOS for iron. This particular model includes four solid phases

(alpha, gamma, epsilon, delta), melting, and vaporization. It agrees well with most experimental data, including impact and penetration experiments and wave profile measurements, which show multiple shock behavior.[16]

Constitutive Equations

When a hydrocode is employed to model material deformation and failure, constitutive models are used to define the equations for the stress and deformation relationships in a material. To solve the high-speed, high-temperature, large-deformation, high-strain-rate gouging problem, advanced models need to be considered that can include these effects. The Johnson–Cook model represents an empirical relationship for the yield stress Y (Ref. 17):

$$Y = [A + B(\varepsilon^p)^n](1 + C \ln \dot{\varepsilon})[1 - (T^*)^m] \tag{4}$$

where A, B, C, n, and m are empirically determined material constants, ε^p is the equivalent plastic strain, and T^* is the homologous temperature $(T - T_r)/(T_m - T_r)$, where T is temperature, T_r is room temperature, and T_M is the melt temperature. This model is essentially a mathematical fit to experimental data. The effective stress σ_{eff} is compared to the yield stress Y. When $\sigma_{\text{eff}} < Y$, the material is totally elastic, and no viscoplastic behavior is consdered. When $\sigma_{\text{eff}} > Y$, the material has entered the viscoplastic region, and the Johnson–Cook model is initiated.

The Steinberg–Guinan–Lund (SGL) model predicts the viscoplastic response of various materials, mostly metals, based on thermally activated dislocation mechanics.[14] This model again compares the effective stress to a yield stress function. The strain rate-dependent form of the SGL model defines the yield stress as

$$Y = \left[Y_T(\dot{\varepsilon}^p, T) + Y_A f(\varepsilon^p)\right][G(P, T)/G_0] \tag{5}$$

where the yield strength at the Hugoniot elastic limit Y_A and the work-hardening function $f(\varepsilon^p)$ comprise the athermal component, Y_T is the thermally activated stress component, G is the shear modulus, T is the temperature, P is the hydrostatic pressure, G_0 is the room temperature and zero-pressure initial shear modulus, and ε^p is the equivalent plastic strain.[18]

Modeling Technique

In addition to the numerical considerations discussed earlier, there are several physical aspects that will affect development of gouging. These include the horizontal and vertical velocities, material properties, initial temperatures, and geometry.

The model scenario is intended to describe the gouging that occurs from hypervelocity sled runs at the Holloman High Speed Test Track. During hypervelocity impact, it should be remembered that geometry could affect the behavior of shock-wave propagation and reflection, which can greatly influence the problem. The initial geometry shown in Fig. 5 is based on the slipper of a high-speed sled. Because CTH is an Eulerian finite volume code, the computational grid remains fixed while the materials pass through it, and all grid locations where calculations will be performed need to be in place at the beginning of the simulation. Figure 5 shows the entire computational space, which is 7.50 cm (2.95 in.) wide and 5.52 cm (2.17 in.) high. It contains a 2.54-cm (1.0-in.)-thick by 4.37-cm (1.72-in.)-long flyer with a 0.2-cm (0.079-in.)-radius chamfer on the leading edge in contact with a target. An actual sled slipper can be up to 8 in. long, but the model was shortened to conserve computational processing time because the gouge initiates near the front of the flyer, and the initiation is currently of more interest than the propagation of the gouge through the entire flyer. The target is modeled as half-space (infinitely deep, infinitely wide). Dictated by the location of the computational boundary on the left, right, and bottom, the part of the target that lies within the computational space is 2.76 cm (1.09 in.) thick by 7.5 cm (2.95 in.) long. The boundary condition on these sides is a sound-speed-based absorbing condition simulating a semi-infinite medium such as a half-space. The remainder of the computational space is void. No calculations are performed for cells containing void until one or more of the materials moves into them.

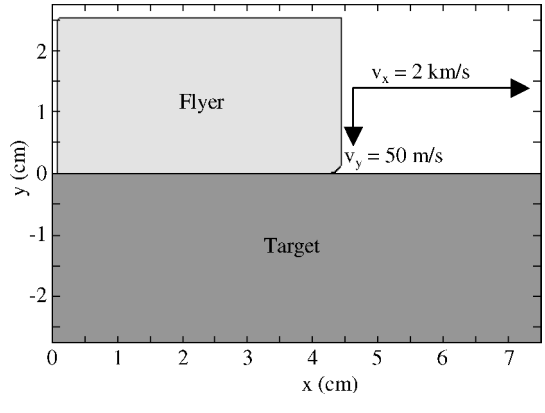

Fig. 5 Oblique impact scenario.

The model is a two-dimensional plane-strain simulation that calculates the conditions along the centerline of the gouge. Experimental gouges are fairly symmetric, and the plane-strain problem simulates conditions along the plane of symmetry.

To initiate an oblique impact event, the flyer is given a horizontal velocity component of 2.0 km/s (6562 ft/s) and a vertical component of 50 m/s (164 ft/s) as initial conditions. The DADS analysis has shown that expected vertical impact velocities range from 2 to 2.5 m/s. However, the flyer mass used in the simulations is much less than the mass of an actual sled. The kinetic energy of a 227-kg (500-lb) sled moving at 1 m/s is equivalent to the model's 89.77 g flyer at 50.26 m/s, which is why 50 m/s was chosen. Because the two materials are already in contact along the flyer length, this initial condition represents the instant that any gap between the two materials is closed and the impact begins.

HHSTT sled slippers are typically constructed of a high strength steel such as VascoMax 300,[19] and so the flyer is modeled using the tabular SESAME EOS for VascoMax 300. Sandia created this EOS using the same EOS for iron but with a density scaling factor. The flyer also uses the Steinberg–Guinan–Lund constitutive model created for VascoMax 250 steel with the yield strength increased to that of VascoMax 300.

The HHSTT rails are made of 1080 steel crane rail. The rail is also usually coated with a primer or epoxy, but such coatings are not modeled in this effort. Coatings, however, greatly increase the gouge threshold velocity at the test track, and the modeling of these has been considered by Schmitz et al.[5] As demonstrated by the Johnson–Cook and Steinberg–Guinan–Lund models, advanced constitutive models typically use certain material properties that are particular to the model and must be determined experimentally with the model in mind. However, no material data for applicable high-strain-rate constitutive equations were available for 1080 steel, and so iron was chosen as a surrogate target material. Even so, Steinberg–Guinan–Lund material data were not available for iron, and so the Johnson–Cook viscoplastic model for iron is used here instead. Similarly, Johnson–Cook material data were not available for the intended flyer material, and so two different constitutive models were used. The target also uses the SESAME iron EOS. A summary of the constitutive model constants used is given in Table 2.

After a study on the effect of grid size, the resulting computational mesh is composed of about 54,000 rectangular cells: the ones near the gouging region being most refined at 0.005 cm on a side, and the coarsest cells near the boundary are 0.08 cm on a side. Further refinement of the mesh does not significantly alter the solution. An additional negative velocity about half of the flyer velocity was imparted to both materials to keep the gouge centered in the region of the most refined cells, but maintained the relative velocity between the flyer and target. This step is the equivalent of moving the grid along follow the gouge.

Methods for Implementing Thermal Environment

To implement elevated temperature models into numerical calculations, three methods of increasing fidelity have been prepared.

Table 2 Material constants

Johnson–Cook target: iron		Steinberg–Guinan–Lund Flyer[a]: VascoMax300	
Model constant	Value	Model constant	Value
ρ_0[b]	7.850 g/cm^3	ρ_0	8.129 g/cm^3
A	1.7526×10^9 g/cm s^2	G_0	7.18×10^{11} g/cm s^2
B	3.8019×10^9 g/cm s^2	Y_0	1.56×10^{10} g/cm s^2
C	0.06	A	2.06×10^{-12} cm s^2/g
n	0.32	B	3.15×10^{-4} 1/K
m	0.55	β	2.0
T_M	1835.7 K	n	0.5
		$Y_{\max}$	2.5×10^{10} g/cm s^2
		γ_0	1.67
		a	1.2
		T_{m0}	2310 K

[a]Constants not listed are zero.
[b]Not used in Johnson–Cook model; listed for reference.

For each of these methods, it is assumed that during the gouging event itself the heating rate from friction or aerodynamics is negligible. This assumption is used because gouging initiates and develops in a matter of microseconds, a much smaller timescale than the diffusion rate of the materials involved. This being the case, the temperature state before the impact is estimated and imposed as an initial condition immediately prior to impact. During the impact event, changes in temperature state as a result of deformation and state changes are still dealt with via the equation of state and conservation equations.

The three methods vary the initial temperature state of the flyer and target. The first method uses a constant temperature in the flyer. The second method uses a distribution. The third method uses the distribution in the flyer, as long as a distribution in the target.

The simplest method used here assumes that the flyer has arrived at a uniform, steady-state temperature equal to the heat sources. Furthermore, the target can be said to be at room temperature because the heat source (moving with the flyer) is at the impact region for too small of a time for heat to be conducted into the target. To establish a possible temperature regime, the test profile in Fig. 3 has been considered. At 3 km/s in helium, the stagnation temperature would be 1200 K. A source strength temperature range of 298 to 2500 K has been examined.

To improve the fidelity of this model, a two-dimensional transient heat-transfer solution is employed within the flyer, considering the effects of stagnation temperature, airflow between the flyer and target, and friction as heat sources. Analytical efforts by Korkegi and Briggs[6,7] show that the heat flux from each of these sources is of similar magnitude. For this reason the sources are assumed to be the same in the model. Because the frictional heating only occurs when the flyer is in contact with the target and is replaced by aerodynamic heating in the gap while not in contact, these sources at the contact surface are treated as only one source that is present throughout the length of the run. This thermal model is simply the flyer with a temperature source along its bottom and front edges.

The variation of temperature with time of a two-dimensional bar is governed by the heat-conduction equation[20]

$$\frac{\partial u}{\partial t} = \alpha\left(\frac{\partial^2 u}{\partial x^2} + \frac{\partial^2 u}{\partial y^2}\right), \qquad t > 0 \tag{6}$$

where α is the thermal diffusivity, defined as

$$\alpha = \kappa/\rho c_v \tag{7}$$

Here, κ is the thermal conductivity, ρ is the density, and c_v is the specific heat of the material.

For VascoMax 300 a maraging steel from which many flyers are made, κ, ρ, and c_v, are temperature dependent. To simplify, these values are taken to be constant, and their values at 700 K (the average temperature during the helium phase of the sample HHSTT run) are

$$\kappa_{700K} = 3.0807 \times 10^6 \text{ g cm/s}^3\text{K}$$

$$c_{v700K} = 8.583 \times 10^6 \text{ cm/s}^2\text{K}$$

$$\rho_{700K} = 7.9173 \text{ g/cm}^3$$

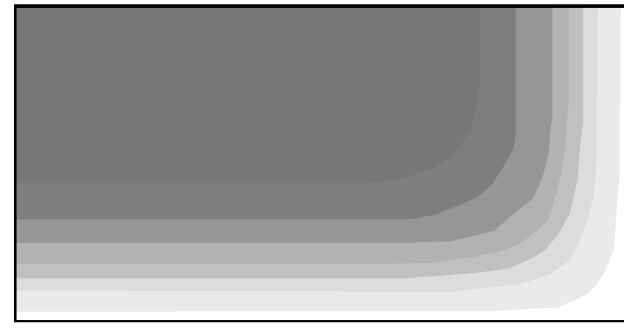

Fig. 6 Time-dependent flyer temperature profile at 5 s.

Using these values in Eq. (7), the thermal diffusivity is

$$\alpha_{700K} = 4.5118 \times 10^{-2} \text{ cm}^2/\text{s}$$

The heat equation can now be solved using a simple finite difference algorithm:

$$u_{i,j}^{n+1} = u_{i,j}^n + \alpha(\Delta t/l^2)\left[\left(u_{i-1,j}^n - 2u_{i,j}^n + u_{i+1,j}^n\right) + \left(u_{i,j-1}^n - 2u_{i,j}^n + u_{i,j+1}^n\right)\right] \tag{8}$$

where u is the temperature; Δt is the time step; l is the length of the finite difference cell; and n, i, and j are the time and spatial indices. Using 735 cells, the resulting temperature profile in the flyer after 5 s is shown in Fig. 6, where white represents the source temperature and each consecutive color contour indicates a drop in temperature. In this case the contact surface is at the source strength temperature, while the temperature drops away from the surface. For the CTH model the flyer contained 10 bands of temperatures, each consecutive band having a 10% drop in source strength. These temperatures are set as initial conditions. When setting the initial temperature of a material in CTH, the EOS package also reads in the initial density and calculates the equilibrium pressure. In this case, for the selected temperature the equilibrium density for zero pressure was looked up in the tabular EOS using BCAT (a companion code to CTH for EOS) and then also used as an initial condition. This method does not capture the internal stresses caused by the thermal gradient.

The third method, further refining the initial temperature model, is to consider temperature in the target as well. Although the heat source is present over the impact area of the target for only a short period of time, analysis of the heat conduction shows that a very shallow heated layer is created. Considering the heated flyer to be the thermal source for target heating, Baker et al.[21] developed a steady-state solution of thermal profiles generated in a target for high-speed sources. A term λ representing the ratio timescales for velocity and diffusion is defined by

$$\lambda = \rho v c_v l/2\kappa \tag{9}$$

where v is the flyer velocity and l is the flyer length. Because the velocity is very high compared to the rate of thermal diffusion,

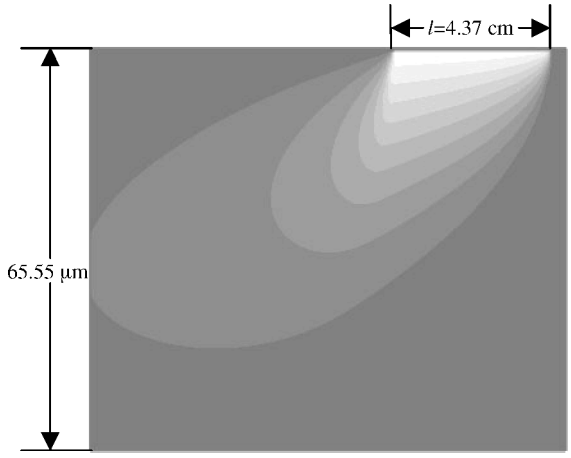

Fig. 7 Steady-state target temperature solution.

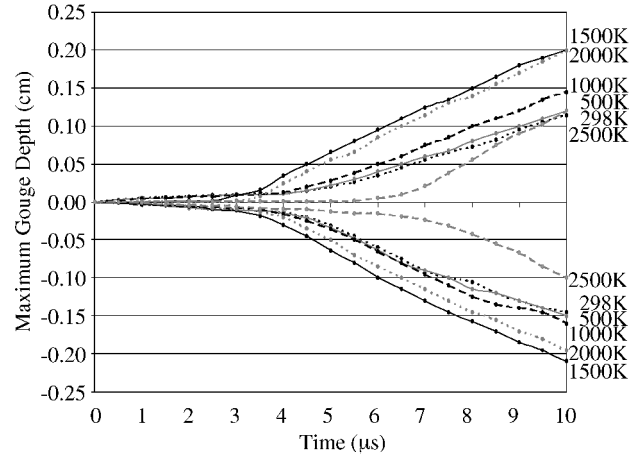

Fig. 8 Maximum gouge depth vs time for various uniform flyer temperatures.

λ is expected to be very large. Then the ratio of the steady-state temperature distribution in the target and the source strength is given by

$$u_{ss}(\xi, \eta) = \frac{\lambda\eta}{\pi} \int_0^1 e^{-\lambda(\xi - \varsigma)} f(\varsigma) \frac{K_1(\lambda R)}{R} \, d\varsigma \qquad (10)$$

where ξ and η are nondimensionalized coordinates attached to the source, ς is the nondimensionalized time, K_1 is the second kind modified Bessel's function of order one, and R is a function of the coordinates.

Determining λ using Eq. (9) and applying the material properties for 1080 steel, the material the HHSTT rail is made from

$$\rho = 7.85 \text{ g/cm}^2, \qquad c_v = 5.024 \times 10^6 \text{ cm}^2/\text{s}^2\text{K}$$

$$l = 4.34 \text{ cm}, \qquad \kappa = 4.774 \times 10^6 \text{ g cm/s}^3\text{K}$$

$$v = 2 \times 10^5 \text{ cm/s}$$

we get

$$\lambda = 3.61 \times 10^6$$

For a unit nondimensionalized source strength, solving Eq. (10) results in the temperature profile displayed in Fig. 7. The actual depth of this profile is very shallow, and the size of the y axis is magnified 2000 times vs the length of the x axis to show detail. Each color shade represents a 10% decrease from the source temperature.

Because the penetration depth of a 10% of the source temperature is less than the size of the smallest computational cell, a worst-case approximation of one cell layer at the target surface was given the source temperature as an initial condition. Because the thermal source is applied to unheated portions of the target so quickly, the described target temperature profile is considered to be a temperature shock. In writing the initial conditions for the target in CTH, this was accomplished by prescribing the elevated temperature to the desired area but retaining the room temperature density. Thermodynamic equilibrium, enforced through the EOS, results in a high initial pressure in these areas.

Results of Elevated, Uniform Temperature Environment

At room-temperature conditions (298 K) gouging generally initiates at the leading edge of contact. The flyer slightly penetrates into the target, developing a horizontal hypervelocity impact at the leading edge of the flyer. Because of the high velocity and the high resulting strain rate, the material in this region begins to exhibit fluid behavior. The plastic flow in this area creates material jets that impinge on each other, creating an increasing area of interaction between the flyer and target. The center of this interaction region moves from its point of origin at the average speed of the two materials or at about half the speed of the flyer. Details of the mechanical process can be found in the papers by Laird et al.[12] and Laird.[13]

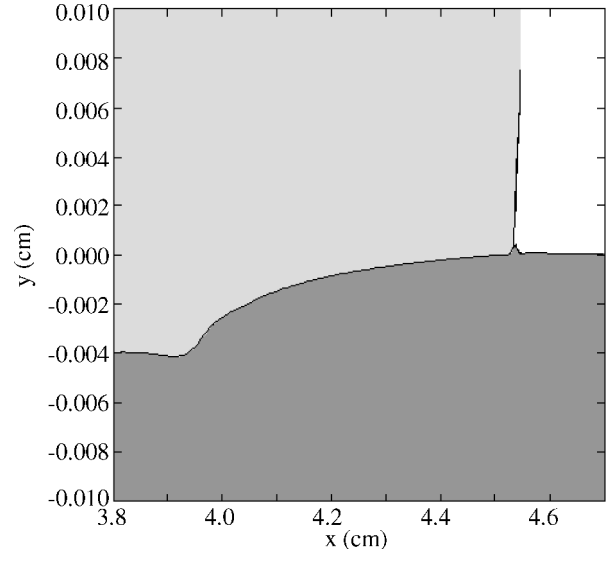

Fig. 9 Gouge initiation with 2500 K flyer at 2.0 μs.

In the material presented, numerical simulations have been performed using source temperatures of 298, 500, 1000, 1500, 2000, and 2500 K. At zero pressure the melting point of the flyer is 2310 K. Considering a flyer with a uniform temperature distribution, representing a steady-state thermal condition, the maximum gouge depth vs time is shown in Fig. 8 for the various temperatures. Compared to the room temperature case at 298 K, as the temperature of the flyer is increased to 500 K there is very little difference in the progression of the maximum gouge depth, except for a very small tendency toward the onset of jet formation beginning sooner and the slope of the high-rate region being slightly steeper. After an increase to 1000 K, the linear growth rates are still similar, and the earlier start of the high-rate onset and the increased slope of the high-rate region become more pronounced, and the trend continues at 1500 K. Further increases to 2000 and 2500 K begin to reverse the trends of the high-rate region. Here, the onset of the higher rate begins to occur more slowly, although the slope remains slightly steeper than at lower temperatures. At 2500 K the onset point of 6.0 μs is even slower than the 4.0 μs onset at room temperature.

After studying the development of gouges at high temperatures, two separate gouge-initiating interactions are apparent. One is at the leading edge, where a small amount of target material is pushed in front of the target. The other is behind the leading edge, where the flyer has penetrated into the target because of the vertical component of the impact. Both cases create a situation where the contact surface of the materials has a horizontal component that can lead to gouging. Figure 9 shows the material interface at 2.0 μs for a 2500 K slipper,

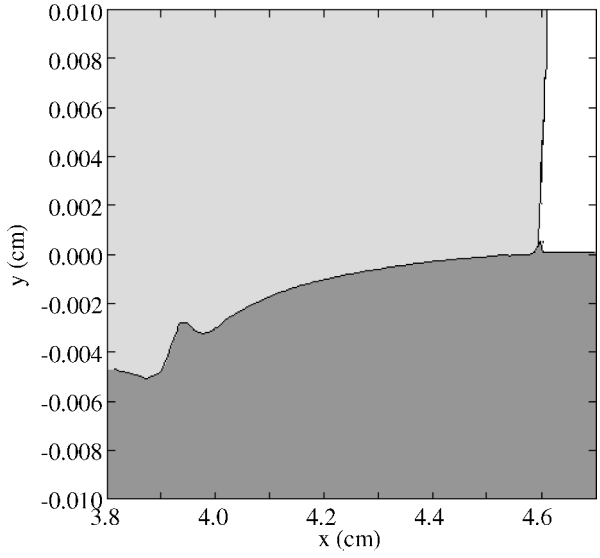

Fig. 10 Gouge initiation with 2500 K flyer at 2.5 μs.

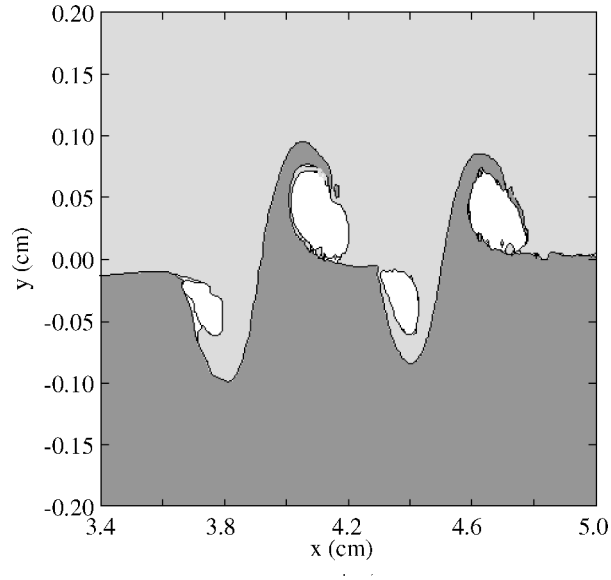

Fig. 11 Double gouges in 2500 K flyer at 23.0 μs.

where it can be seen that a very small amount of the target has been deformed in front of the flyer leading edge, and about 0.6 cm behind the leading edge the flyer has penetrated 0.004 cm into the target. By 2.5 μs the latter penetration has taken the form of a gouge-initiating instability as seen in Fig. 10. The continuing interaction at the leading edge then develops into a gouge several microseconds later, resulting in multiple gouges. As the gouges grow larger than the distance between them, they will coalesce into a single gouge.

Over the temperature range studied, both these gouge-initiating mechanisms are present and are colocated at the moment of impact but differ in their movements after impact. The interaction at the leading edge remains at the leading edge, moving at the speed of the flyer, until it is large enough to initiate a gouge. Once the gouge is formed, its center travels about half the speed of the flyer in the same direction, which can be thought of as the average velocity of the two materials. The material interaction caused by the initial penetration of the flyer into the target (as seen on the left in Fig. 9) also begins at the leading edge but then moves along the target at a rate that is near half of the flyer velocity but decreases with temperature. At room temperature the penetration interaction moves at the same speed as the leading-edge interaction, and the two phenomena occur together, initiating a single gouge. At higher temperatures, however, the penetration interaction tends to move slower. Figure 10 shows that at 2500 K the x location of the penetration-initiated instability ($x = 3.95$ cm) is actually behind the original location of the leading edge at impact ($x = 4.25$).

In addition to the separation of the two initiating mechanisms, the higher temperatures also delay the onset of the leading-edge gouge and accelerate the onset of the penetration gouge. Therefore as the flyer temperature increases, the penetration gouge initiates sooner than the leading-edge gouge. Because the size of a gouge increases with time, the size of multiple gouges with respect to each other depends on when they initiate. In the case of the 2500 K flyer, the leading-edge gouge is delayed enough that the penetration-induced gouge is always larger. Figure 11 shows fully developed double gouges at 2500 K, where the leeward gouge, having been the first initiated, is larger than the leading gouge. In this figure the y direction is magnified to show gouge detail, and the white areas are voids that have opened between the materials. But at 1500 K the two gouges initiate at similar times and develop at similar rates. This double gouging is shown at 6 μs in Fig. 12, also magnified in the y direction.

Gouging can be described as a surface layer mixing of the two materials. Although fluidlike motion and fluid mixing can be seen at low temperatures, it becomes more pronounced as the temperature is increased. Figure 13 shows details of the flyer/target mixing at 1500 K caused by a double gouge.

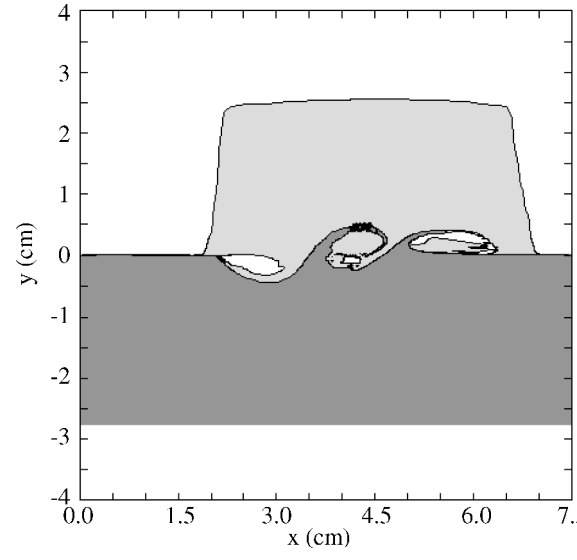

Fig. 12 Double gouge formation in 1500 K flyer at 6.0 μs.

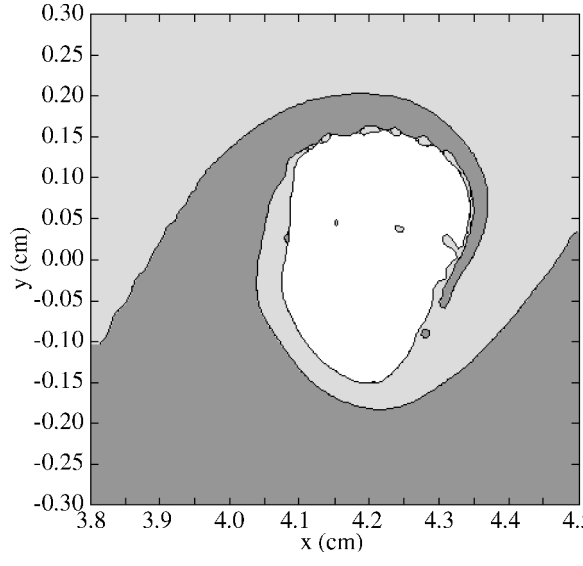

Fig. 13 Material mixing for 1500 K flyer at 10 μs.

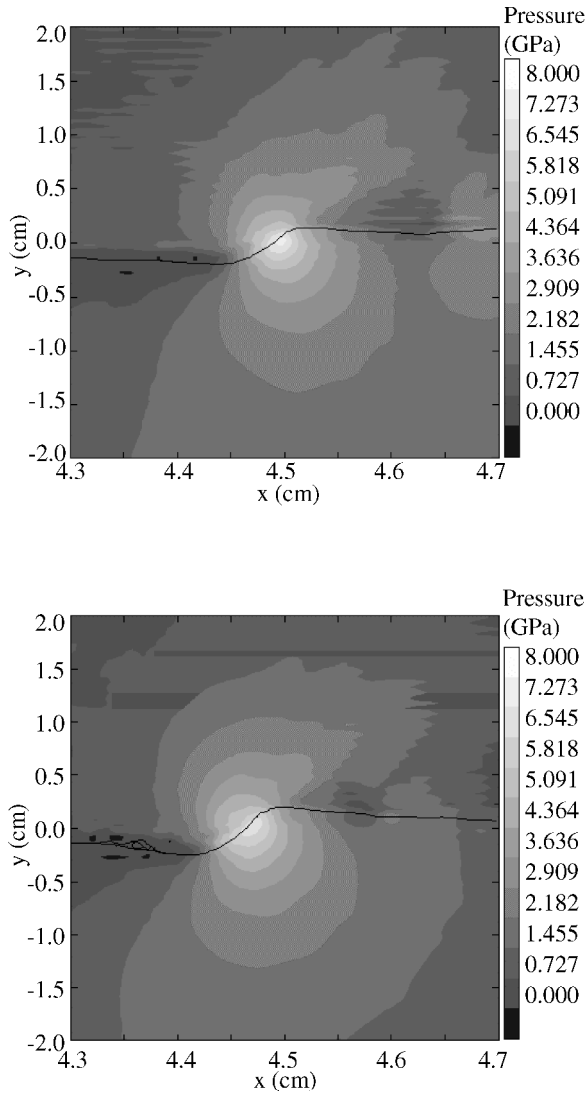

Fig. 14 Pressure profile at 4.5 μs for flyer initially at 298 K (left) and 1000 K (right).

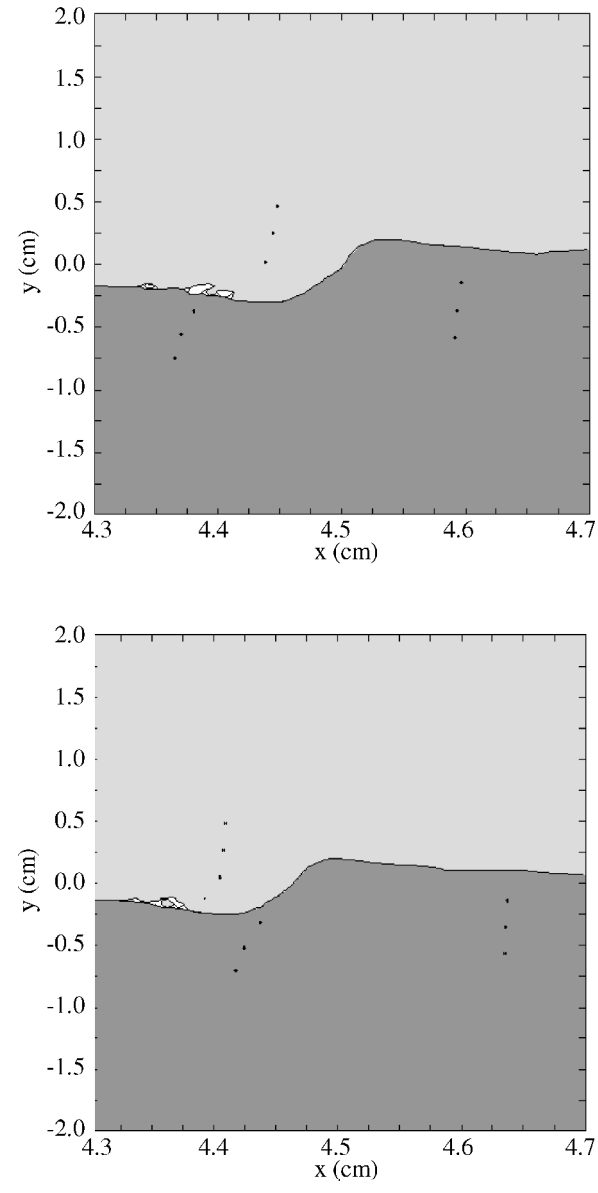

Fig. 15 Material plots for 298 K flyer at 5.0 μs (left) and 1000 K flyer at 4.5 μs (right).

Figure 14 shows a comparison of pressure profiles between the 298 K case and 1000 K case at 8.0 μs. At 298 K the high-pressure region is smaller in size, but at about 8 GPa (1160 ksi) it is of a slightly higher magnitude than the 1000 K case. It can also be seen that the higher-temperature case has a larger gouge. An interesting point is that the higher temperature has the effect of accelerating the growth of the gouge. At 5.0 μs the lower-temperature gouge will have a similar size and shape and will be just starting flyer jet formation as the 1000 K sample has at 4.5 μs as in Fig. 15.

The resulting temperature at 4.5 μs for both the 298 and 1000 K cases is shown in Fig. 16. In the 298 K case all heating is caused by shock and strain heating. In the 1000 K case, although the flyer is at an elevated temperature, the maximum temperature is similar to that for the 298 K case, about 1500 K (2240 °F). Higher temperatures lower the yield stress of the materials, leading to less resistance to gouging. While the room temperature gouge has reached higher temperatures contributing to weakening of the material, the heated flyer provides a jump-start to reaching higher temperatures, leading toward similar behavior and deformation as the unheated case, but at an earlier time.

The effect of the flyer temperature on yield stress can be seen in Fig. 17. Here, the yield stress of the materials at 4.5 μs is shown at both 298 and 1000 K. The materials generally have a higher than normal yield stress because they have been work hardened by the initial plastic stress wave and deformation in the interaction region. Although very little difference is seen in the target, the yield stress of the flyer is decreased overall because of the increased temperature, as expected.

Clearly, elevated flyer temperatures affect the onset and subsequent development of gouging. Even as low as 500 K, the higher temperature aids in the initiation of gouges and accelerates their growth. Above 1500 K growth is further accelerated; however, initiation is delayed.

Flyer Temperature Profiles and Elevated Target Temperature

To improve upon the sophistication of the temperature environment, a time-dependent flyer temperature profile has also been implemented as described earlier. With a 500 K source temperature there is very little difference between the three cases of uniform flyer, time-dependent flyer profile, and flyer profile with target temperature, as shown in Fig. 18. At 1000 K there is also no change, and at 1500 and 2000 K results for all three cases are still very similar. This indicates that the use of a temperature profile does not affect gouge development below 2000 K and that only the conditions within 0.1 cm of the surface significantly affect the gouge. But these results also show that the target temperature, confined to within

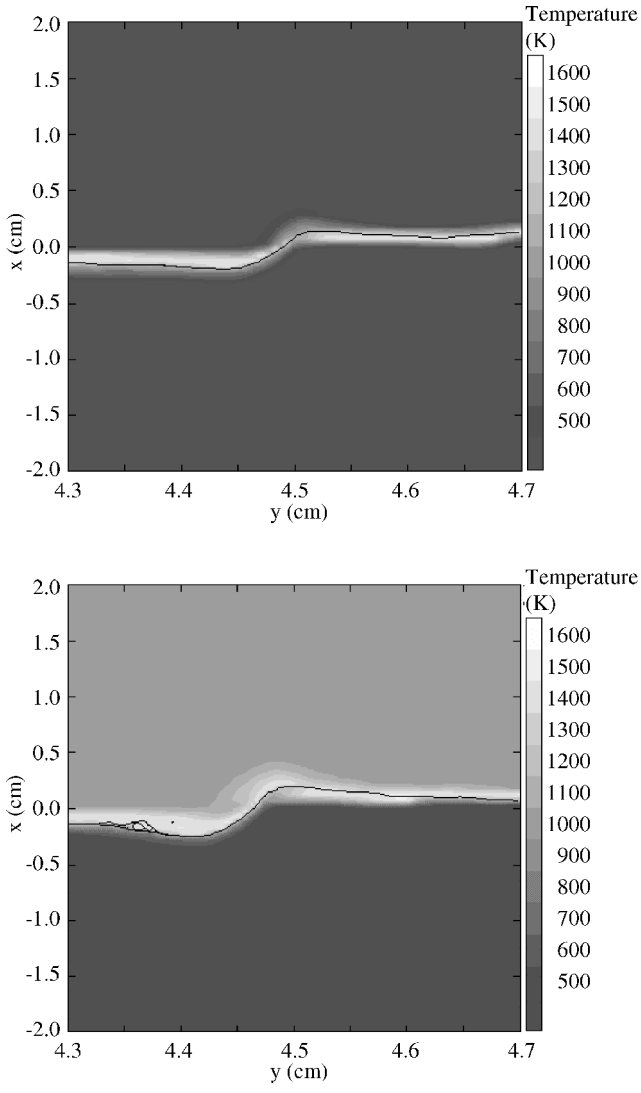

Fig. 16 Temperature profile at 4.5 μs for flyer initially at 298 K (left) and 1000 K (right).

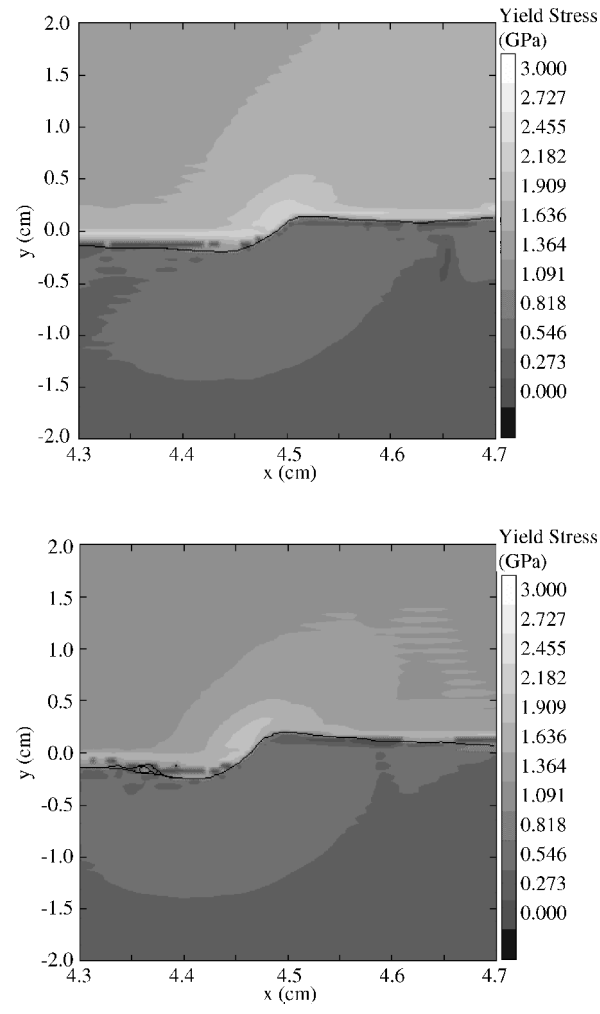

Fig. 17 Yield stress at 4.5 μs for flyer initially at 298 K (left) and 1000 K (right).

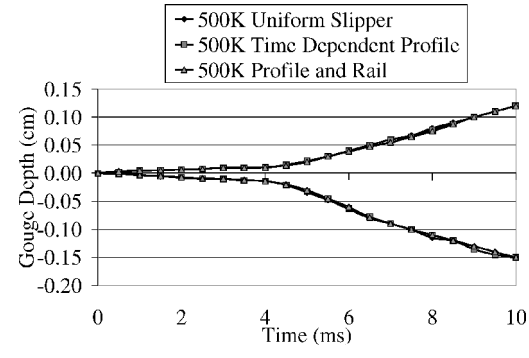

Fig. 18 Maximum gouge depth vs time for 500 K source temperature.

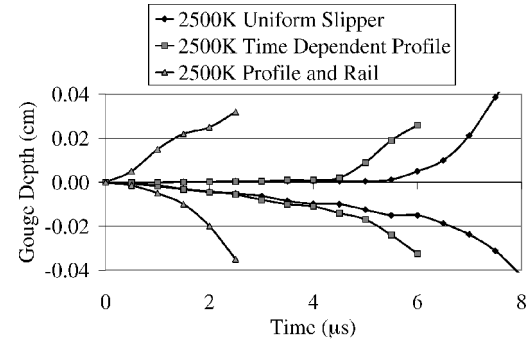

Fig. 19 Maximum gouge depth vs time for different thermal enviornments with a 2500 K source strength.

0.005 cm of the surface, did not have any effect. Either the layer was too thin to influence events, or altering the target at this point does not change anything. Gouging involves interaction and mixing between two materials. Because gouging is dependent on the plasticity of both materials, if one material has conditions or properties that prevent it from participating in gouging gouging will not occur, even if the other material has conditions or properties that allow it to gouge. In this case it might be that the flyer is the material most resistant to gouging, and so creating conditions that make the target more susceptible (such as heating it) makes little or no difference.

At 2500 K the situation changes, and all three temperature environments produced different results. Using the temperature profile in the flyer caused gouging to initiate a microsecond sooner that the uniform flyer, as shown in Fig. 19. This temperature is above the melting point of both the flyer and target materials. In the uniform temperature case the flyer material is completely melted. In the case of the flyer profile, only the surface is melted, whereas the interior is still solid.

Using the flyer profile in conjunction with the target temperature resulted in immediate gouging. This is primarily because at 2500 K the pressure in the target is so great that it causes the target to rise upward so much and so rapidly that the flyer impacts this part of the target horizontally sooner than horizontal impact would have developed as a result of target surface penetration.

Conclusions

The initial temperature state of a flyer/target system in a sliding impact scenario has been determined analytically and implemented as an initial condition to a numerical gouging simulation. The initial temperature profiles are highly dependent on assumptions made about the heat source. Based on the constitutive equations used, it is expected that the yield stress will be decreased, and this is likely to increase the tendency to gouge.

Successful modeling of gouging should include modeling the temperature environment, as the flyer temperature has proven to have a significant affect on the material yield stress and its resistance to gouging. As the flyer temperature increases above ambient temperature, the tendency is that gouging initiates sooner and grows faster during an oblique impact, until the temperatures approach the melting temperature, where the onset of gouging begins to get delayed. Higher temperatures lower the yield stress of the materials, leading to less resistance to gouging. Even as low as 500 K, the higher temperature aids in the initiation of gouges and accelerates their growth. Detail of the temperature environment has proven to be not as important. Inclusion of a thermal profile or target temperature did not significantly influence events until the source temperature was above the melting temperature.

Elevated temperatures affect the mechanism of gouge initiation. At room temperature the gouge develops at a location based on the small target hump initially at the leading edge of the flyer. At high temperatures however, multiple gouges are observed, some of which develop away from the leading edge at a point where flyer penetration caused by the vertical component of impact is the greatest. At the temperatures studied between 298 and 2500 K, both these mechanisms are present. At the start time these phenomena are colocated near the leading edge. The leading-edge instigated interaction always moves along the target at the same speed independent of temperature. At lower temperatures the penetration interaction moves at the same speed, and the two phenomena occur together. At higher temperatures, however, the penetration interaction tends to move along the target more slowly, physically separating the two mechanisms. The higher temperatures hinder the initiation of the leading-edge gouge, whereas initiation of the penetration gouge is accelerated by it, except for the 2500 K case, which is above the melting point of the flyer, where the initiation of both gouges are delayed.

Acknowledgments

This research is sponsored by the U.S. Air Force Office for Scientific Research with Len Sakell as Program Manager. The authors acknowledge the input and assistance of William Baker, Craig Schmitz, Michael Hooser, and David Belk. The views expressed in this article are those of the authors and do not reflect the official policy or position of the U.S. Air Force, Department of Defense, or U.S. Government.

References

[1]Barker, L. M., Trucano, T. G., and Susoeff, A. R., "Railgun Rail Gouging by Hypervelocity Sliding Contact," *IEEE Transactions on Magnetics*, Vol. 25, No. 1, 1989, pp. 83–87.

[2]Barker, L. M., Trucano, T. G., and Munford, J. W., "Surface Gouging by Hypersonic Sliding Contact Between Metallic Materials," Sandia National Labs., SAND87-1328-UC-34, Albuquerque, NM, 1987.

[3]Tachau, R. D. M., "An Investigation of Gouge Initiation in High-Velocity Sliding Contact," Sandia National Labs., SAND91-1732-UC-706, Albuquerque, NM, 1991.

[4]Tarcza, K. R., "The Gouging Phenomenon at Low Relative Sliding Velocities," M.S. Thesis, Univ. of Texas, Austin, TX, 1995.

[5]Schmitz, C. P., Palazotto, A. N., and Hooser, M. D., "Numerical Investigation of the Gouging Phenomena Within a Hypersonic Rail/Sled Assembly," AIAA Paper 2001-1191, 2001.

[6]Korkegi, R. H., and Briggs, R. A., "Aerodynamics of Hypersonic Flyer Bearing," Aerospace Research Lab., ARL 68-002, 1968.

[7]Korkegi, R. H., and Briggs, R. A., "The Hypersonic Flyer Bearing—A Test Track Problem," *Journal of Spacecraft and Rockets*, Vol. 6, No. 2, 1969, pp. 210–212.

[8]Lofthouse, A. J., Hughson, M. C., and Palazotto, A. N., "Hypersonic Test Sled External Flow Field Investigation Using Computational Fluid Dynamics," AIAA Paper 2002-0306, Jan. 2002.

[9]Krupovage, D. J., and Rassmussen, H. J., "Hypersonic Rocket Sled Development," Test Track Div., AD-TR-82-41, Holloman AFB, NM, 1982.

[10]Mixon, L. C., "Assessment of Rocket Sled Flyer Wear/Gouging Phenomena," *Flyer Wear and Gouging Phenomena*, ARA SBIR Rept. 846 TS/TGTAD by T. Caipen and C. Needham, 1997, Chap. 4.

[11]Schoenfeld W. P., "Requirements for Upgrading the Holloman High Speed Test Track Computational Fluid Dynamics Analytical Capability," *Proceedings of the 21st AIAA Advanced Measurement Technology and Ground Testing Conference*, AIAA, Reston, VA, 2000.

[12]Laird, D. J., Palazotto, A. N., and Hooser, M. D., "High Speed Test Track Flyer/Rail Gouging Phenomena Simulations," *Thermal Hydraulics, Liquid Sloshing, Extreme Loads, and Structural Response*, edited by F. J. Moody, PVP-Vol. 421, American Society of Mechanical Engineers, 2001, pp. 61–68.

[13]Laird, D. J., "The Investigation of Hypervelocity Gouging," Ph.D. Dissertation, U.S. Air Force Inst. of Technology, AFIT/DS/ENY/02-01, Wright–Patterson AFB, OH, March 2002.

[14]McGlaun, J. M., and Thompson, S. L., "CTH: A Three-Dimensional Shock Wave Physics Code," *International Journal of Impact Engineering*, Vol. 10, 1990, pp. 351–360.

[15]Anderson, C. E., Jr., "An Overview of the Theory of Hydrocodes," *International Journal of Impact Engineering*, Vol. 5, 1987, pp. 33–59.

[16]Kerley, G. I., "Multiphase Equation of State for Iron," Sandia National Labs., SAN93-0027 · UC-410, Albuquerque, NM, 1993.

[17]Holmquist, T. J., and Johnson, G. R., "Determination of Constants and Comparison of Results for Various Constitutive Models," *Journal de Physique IV*, Colloque C3, suppl. to *Journal de Physique III*, Vol. 1, 1991, pp. C3:853–C3:860.

[18]Computational Physics Research and Development Dept., "ALEGRA: User Input and Physics Descriptions," Sandia National Labs., Albuquerque, NM, 1999.

[19]Hall, A. M., and Slunder, C. J., "The Metallurgy, Behavior, and Application of the 18-Percent Nickel Maraging Steels," NASA SP-5051, 1968.

[20]Boyce, W. E., and DiPrima, R. C., *Elementary Differential Equations and Boundary Value Problems*, Wiley, New York, 1992.

[21]Baker, W. P., Palazotto, A. N., and Laird, D. J., "Thermal Diffusion from a High Speed Source Moving Along a Rail," *Journal of Aerospace Engineering* (to be published).

E. Oran
Editor-in-Chief